

Article

Study on Mechanical and Flow Properties of Cemented Sulfur Tailings Backfill Considering the Influence of Fiber Type, Fiber Content and Addition Method

Wei Liu, Shenghua Yin *, Yongqiang Hou and Minzhe Zhang

School of Civil and Resource Engineering, University of Science and Technology Beijing, Beijing 100083, China; b20180042@xs.ustb.edu.cn (Y.H.)

* Correspondence: hyq2428204462@163.com; Tel.: +86-010-62333152

Abstract: Previous studies have confirmed that for cemented tailings backfill, mechanical properties are improved through the addition of fiber. However, for fiber-reinforced cemented sulfur tailings backfill (FRCSTB), physical and flow properties are still unknown. In this paper, the changes in fluidity, splitting tensile strength (STS) and uniaxial compressive strength (UCS) of cemented sulfur tailings backfill (CSTB) are analyzed in detail. Secondly, regarding the addition of glass fiber and polypropylene fiber, the changes in the fluidity, STS and UCS of the CSTB, resulting from the fiber length, fiber content and method of fiber addition used, were analyzed. Moreover, the relationship between the UCS and fiber content is established. Finally, the mechanism behind the influence of fiber and sulfur content on the mechanical properties of CSTB is revealed. The results indicate that with the increase in sulfur content, the fluidity of the tailings slurry exhibits exponential growth. During the process of increasing sulfur content, the UCS and STS of CSTB initially increase and then decrease, reaching maximum values at 12% sulfur content. Similarly, at a fiber content of 0.6%, the UCS and 28d STS of CSTB reach their maximum values. In terms of enhancing the mechanical properties of CSTB, the effectiveness of glass fibers surpasses that of polypropylene fibers. In addition, regarding the improvement of the UCS of CSTB, the mixed addition of fibers is obviously worse than that of fiber alone. However, in terms of enhancing the STS of CSTB, the mixed addition of fibers outperforms the single addition of polypropylene fiber. From a microscopic perspective, polypropylene and glass fiber are able to form strong cohesion with the cement–tailings matrix and effectively prevent the formation and expansion of pores and cracks.

Keywords: polypropylene fiber; glass fiber; sulfur tailings; mechanical properties; flow performance; microstructure characteristic; compressive strength; splitting tensile strength



Citation: Liu, W.; Yin, S.; Hou, Y.; Zhang, M. Study on Mechanical and Flow Properties of Cemented Sulfur Tailings Backfill Considering the Influence of Fiber Type, Fiber Content and Addition Method. *Minerals* **2023**, *13*, 1105. <https://doi.org/10.3390/min13081105>

Academic Editors: Haiqiang Jiang, Liang Cui, Nan Zhou, Xiwei Zhang and Abbas Taheri

Received: 29 June 2023

Revised: 4 August 2023

Accepted: 8 August 2023

Published: 20 August 2023



Copyright: © 2023 by the authors. Licensee MDPI, Basel, Switzerland. This article is an open access article distributed under the terms and conditions of the Creative Commons Attribution (CC BY) license (<https://creativecommons.org/licenses/by/4.0/>).

1. Introduction

Pyrite or its associated minerals constitute a significant mineral resource; however, pyrite mining operations generate substantial quantities of sulfur tailings. The presence of sulfide causes oxidation reactions to produce a certain amount of acidic liquid. Moreover, sulfur tailings are stacked on the surface, which results in pollution to the environment and adversely affects the stability of the tailings dam [1,2]. Currently, the main mining methods include the caving method, the open stope method, and the backfill mining method. Among these mining methods, the backfill mining method plays a dominant role in orebody recovery. This method can not only safely and efficiently recover underground orebody resources but also can effectively deal with the environmental pollution caused by sulfur tailings [3,4]. When preparing suitable backfill, attention should be paid to the transportability of the material and the maintenance of the specified strength characteristics [5]. Meanwhile, research findings indicate that the presence of sulfide within the tailings exerts a significant impact on the uniaxial compressive strength (UCS) of the backfill, resulting in internal crack propagation during later stages [6,7].

Extensive research has been conducted by both domestic and international scholars on the topic of cemented sulfur tailings backfill (CSTB). Yin et al. [8] concluded that during the process of sulfur content increasing, the fluidity of sulfur tailings slurry showed an exponential growth trend but failed to clarify how the fluidity of sulfur tailings slurry is affected by the fiber type and fiber addition method. Chen et al. [9] discovered that sulfur-containing tailings facilitate the early strength development of backfill but failed to reveal the change characteristics of the long-term compressive strength of fiber-reinforced cemented sulfur tailings backfill (FRCSTB). Zeng et al. [10] pointed out that plant ash can effectively inhibit the oxidation of sulfur-containing minerals, and the effect is higher than that of traditional alkaline minerals (volcanic ash, limestone and fly ash). Jiang et al. [11] emphasized that augmenting mass concentration and cement content can effectively alleviate the late strength deterioration of CSTB but ignored the influence of fiber on the mechanical characteristics of CSTB. Ayora et al. [12] noted that when tailings contain pyrrhotite, excessive amounts of secondary gypsum and ettringite are formed, leading to strength deterioration. Yin et al. [13] conducted an analysis to examine how the sulfur content affects the failure process of the backfill. Their findings revealed that, for the backfill's later-stage strength, it continuously decreases as the sulfur content increases. Dong et al. [14] observed a significant correlation between the long-term UCS and sulfur content of backfill but failed to reveal the evolution law of long-term compressive strength. Furthermore, due to the complex geological conditions surrounding the orebody, it is subject to various external disturbances, which inevitably lead to damage to the backfill structure. Therefore, in view of the special environment in which the orebody is recovered, there is an urgent need to explore the mechanical properties of the CSTB.

In recent years, fiber-reinforced technology has been receiving increasing attention [15,16]. The addition of activators to tailings is an activation treatment method that enhances the rheological properties and strength of the backfill material [17,18]. The findings demonstrate that the incorporation of fibers contributes to the overall structural integrity, thereby facilitating the enhancement of concrete's overall stability [19,20]. Xu et al. [21] emphasized that fiber incorporation could effectively inhibit the deformation of backfill, but failed to analyze the mechanism of how fiber addition methods and fiber types affects the mechanical characteristics of the backfill. Chen et al. [22] emphasized the ductility and UCS of the backfill both increase with the increase in polypropylene fiber content. However, they failed to clarify how different fiber types affects the mechanical characteristics of the backfill. Yi et al. [23] highlighted that the inclusion of fiber enhanced the strength of backfill material and avoided the reduction of post-peak strength. Zhou et al. [24] emphasized that adding glass fiber could enhance the shear, tensile and compressive strength of the cemented backfill. Xue et al. [25] observed that the variation and damage of the backfill is restrained by adding fiber, due to its strengthening effect on the mechanical properties of the backfill. Nevertheless, they also ignored the impacts of different fiber types and addition methods on the mechanical properties. Despite numerous studies conducted by both domestic and international scholars on the mechanical properties of CSTB and FRCSTB, the influence of fiber addition method, fiber content and fiber type on the physical and flow properties (slump or fluidity) of CSTB has been overlooked.

Hence, this study focuses on investigating the FRCSTB. Through the experimental research on the physical and flow properties of FRCSTB, a systematic analysis of the effects of varying fiber content, type, and addition method on its properties can be performed. This analysis allows for the identification of the optimal fiber type and content, thereby offering technical guidance for the preparation of high-performance CSTB at the mine site. Moreover, based on scanning electron microscope (SEM) analysis, the mechanism through which fibers enhance the strength of CSTB is elucidated at the microstructural level.

2. Experimental Materials and Methods

2.1. Experimental Materials

Figure 1 illustrates the results obtained from the particle size analysis conducted on the tailings. An XRF spectral analyzer (PRECISE Inc., Shenzhen, China) was used to analyze the chemical composition of the filling material (JINCHUAN GROUP Co., Ltd., Jinchuan, China), and the chemical composition of the material was then revealed. The chemical composition of sulfur concentrate is listed in Table 1. Table 2 [8] displays the chemical composition of tailings and cement. The type of cement is Yunyan ordinary Portland cement, labeled P.C.32.5. Moreover, Table 3 presents the mechanical parameters of the polypropylene and glass fibers (TONGYINGXINCAILIAO Inc., Taian, China). In Table 3, polypropylene fiber and glass fiber are shown to have a high tensile strength and elastic modulus, indicating that the two kinds of fibers have good physical and mechanical properties.

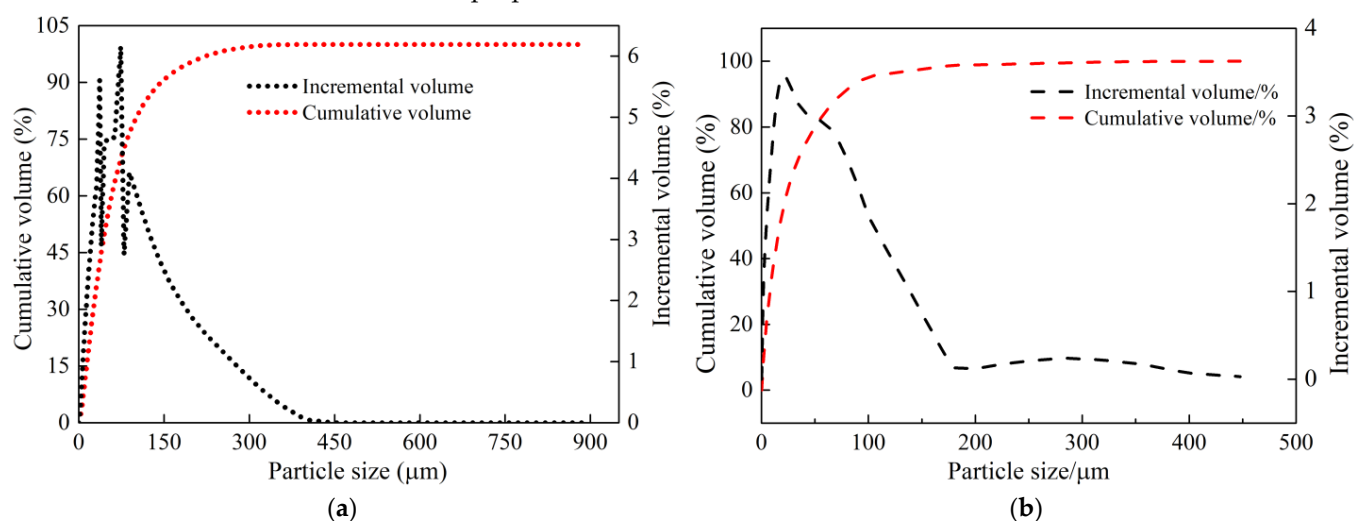


Figure 1. Particle size distribution of sulfur concentrate and tailings: (a) sulfur concentrate; (b) tailings.

Table 1. Chemical composition of sulfur concentrate (mass fraction), %.

Ingredient	C	O	Si	Ca	Fe	S	Cu	Mg	Others
sulfur concentrate	1.07	26.70	2.86	2.09	35.8	27.0	0.35	1.22	2.91

Table 2. Chemical composition of cement and tailings (mass fraction), %.

Ingredient	SiO ₂	CaO	MgO	Al ₂ O ₃	Fe ₂ O ₃	K ₂ O	TiO ₂	MnO	Others
Tailings	42.20	3.73	32.71	4.04	12.14	0.39	0.33	0	4.22
cement	28.36	48.28	2.50	11.87	2.88	1.07	0.60	0.12	4.31

Table 3. Physical and mechanical parameters of polypropylene and glass fibers.

Fiber Type	Diameter/μm	Tensile Strength/MPa	Elastic Modulus/GPa	Density/(g/m ³)	Elongation Rate
Polypropylene	19	350	3.5	0.91	28%
Glass fiber	19	369	4.8	0.91	36.5%

2.2. Experimental Scheme and Preparation of CSTB Specimens

In this experiment, a single-factor test method was employed, and the cement-to-tailings (c/t) ratio was set at 1:8, with a 73% slurry mass concentration, according to the filling body ratio parameter currently used in the mine. Additionally, the sulfur content

was considered the independent variable. According to the mass fraction of the sulfur element in the chemical composition of sulfur concentrate, sulfur concentrate was used to replace part of common tailings to produce sulfur tailings, with a sulfur content ranging from 6% to 25%. Table 4 presents the experimental scheme, in which groups T1 to T4 represent cemented sulfur tailings backfills with different sulfur contents. In addition, some studies [8,9] have shown that the long-term strength of CSTB deteriorates when the sulfur content exceeds 10%. Therefore, the CSTB with an 18% sulfur content (T3 group) was modified by adding polypropylene fiber and glass fiber of different contents and lengths. The fiber length was 3 mm and 12 mm, and the fiber contents (mass fraction) were designed to be 0.2%, 0.4%, 0.6% and 0.8%, based on the research findings of Dong et al. [14] and Cao et al. [26], which indicates that fibers contribute to an enhancement in the UCS within the fiber content range from 0.25% to 0.75%. Therefore, in this experiment, the fiber content was set between 0.2% and 0.8%. In addition, when the glass fibers and polypropylene fibers were mixed, the length of the two types of fibers were fixed at 12 mm. The mixed addition design, encompassing glass fiber and polypropylene fiber, is presented in Table 5.

Table 4. Designed scheme for the experiments.

Serial Number	Slurry Mass Concentration/%	Cement-to-Tailings Ratio	Sulfur Tailings	Sulfur Content/%	Fiber Length/mm	Fiber Content/%
A1	73	1:8	T1	6	/	/
A2	73	1:8	T2	12	/	/
A3	73	1:8	T3	18	/	/
A4	73	1:8	T4	25	/	/
B1	73	1:8	T3	18		0.2
B2	73	1:8	T3	18	3	0.4
B3	73	1:8	T3	18		0.6
B4	73	1:8	T3	18		0.8
B5	73	1:8	T3	18		0.2
B6	73	1:8	T3	18	12	0.4
B7	73	1:8	T3	18		0.6
B8	73	1:8	T3	18		0.8
C1	73	1:8	T3	18		0.2
C2	73	1:8	T3	18	3	0.4
C3	73	1:8	T3	18		0.6
C4	73	1:8	T3	18		0.8
C5	73	1:8	T3	18		0.2
C6	73	1:8	T3	18	12	0.4
C7	73	1:8	T3	18		0.6
C8	73	1:8	T3	18		0.8

Table 5. Design scheme of fiber mixing and adding.

Serial Number	Sulfur Tailings	Sulfur Content/%	Polypropylene Fiber Content/%	Glass Fiber Content/%	Fiber Length/mm
D1	T3	18	0.2	0.2	
D2	T3	18	0.2	0.4	12
D3	T3	18	0.4	0.2	
D4	T3	18	0.4	0.4	

Table 4 [8] presents the weights of sulfur tailings, cement, fibers and water. The specific operation procedure was performed as follows. Initially, the sulfur tailings and cement were mixed, and the materials were stirred for 5 min using a Comex high-speed mixer at a mixing speed of 680 r/min. Simultaneously, during the stirring process, the fibers were gradually added to the material in small portions (dry mixing method). After achieving a thorough dispersion of the fibers, water was added, and the mixture was stirred for 5 min

to prepare the tailings slurry. After measuring the fluidity of slurry, a cylindrical plastic mold (with a diameter of 50 mm and heights of 100 mm) was used to prepare the sample. Considering that the temperature and humidity in the stope of the mine were 25 °C and 95%, respectively, the prepared backfill was placed in a curing box where the humidity and curing temperature were set to 95% and 25 ± 1 °C. When the samples reached the corresponding curing age, the UCS at 7 days, 14 days, 28 days and 56 days and the STS at 28 days were tested. The analysis of each set of samples was repeated three times, and the average value was regarded as the test result. Therefore, 15 samples needed to be prepared for each group of tests, and 360 samples needed to be prepared in total.

The polypropylene fiber, glass fiber and some CSTB samples used in this experiment are shown in Figures 2 and 3. In Table 4, samples numbered B1~B8 and C1~C8 had additions of polypropylene fiber and glass fiber, respectively.

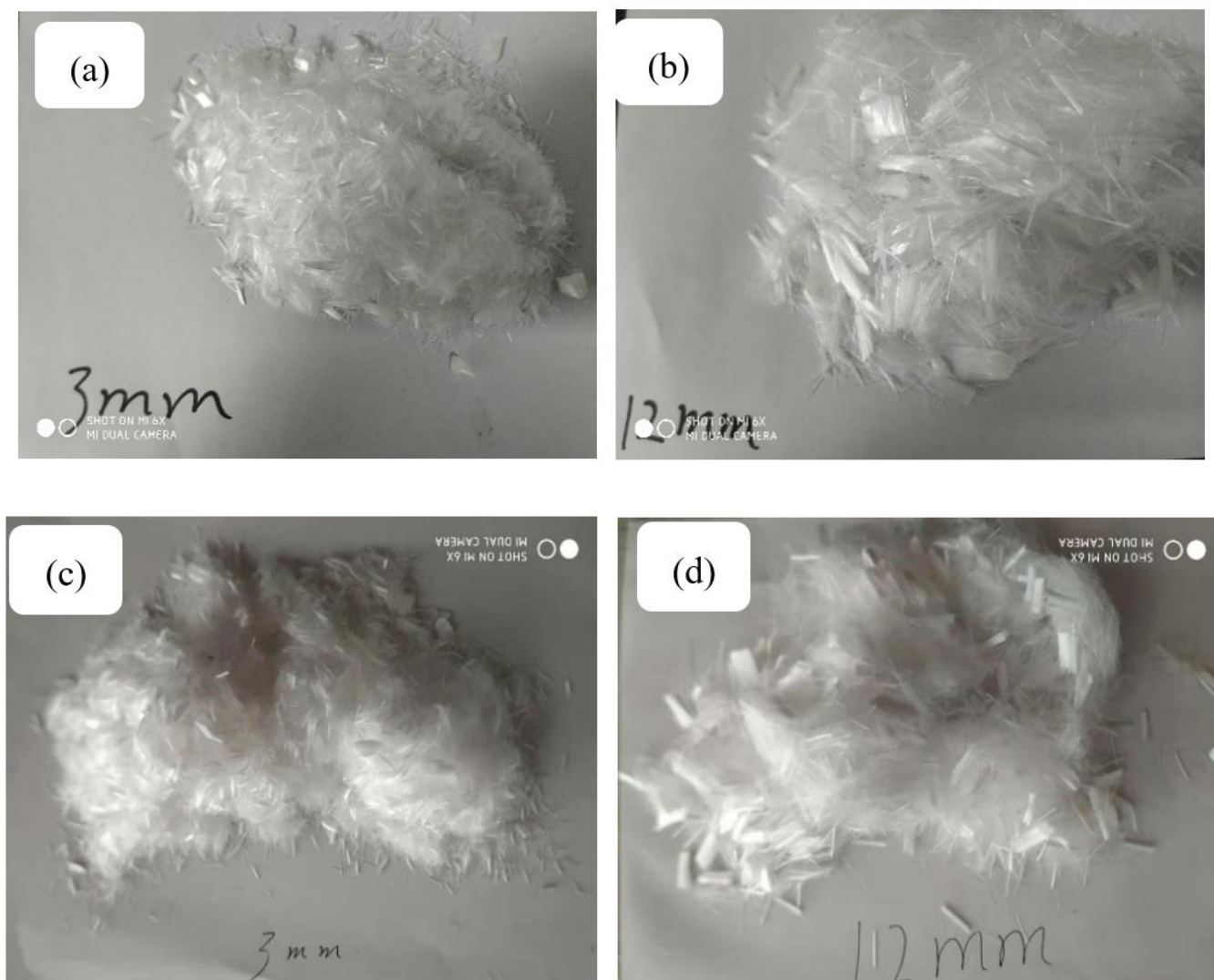


Figure 2. The fibers used in the experiment: (a) Polypropylene—3 mm length; (b) Polypropylene—12 mm length; (c) Glass—3 mm length; (d) Glass—12 mm length.

2.3. Testing Methods

The dimensions of the specimen for uniaxial compression were 50 mm in diameter and 100 mm in height. Figure 4 shows the loading equipment for this experiment. The loading equipment model used was WDW-50 (Beijing Time High Technology Ltd., Beijing, China), which is a microcomputer-controlled electronic universal testing machine, with a loading rate set at 0.05 mm/s. Samples with curing ages of 7, 14, 28 and 56 days were

selected, and their respective compressive strength was assessed following the guidelines outlined in the “Standard of Mechanical Properties test method for Ordinary Concrete” (GB/T 50081-2002). For each group, three samples were selected for testing, and the average compressive strength of each sample was calculated.

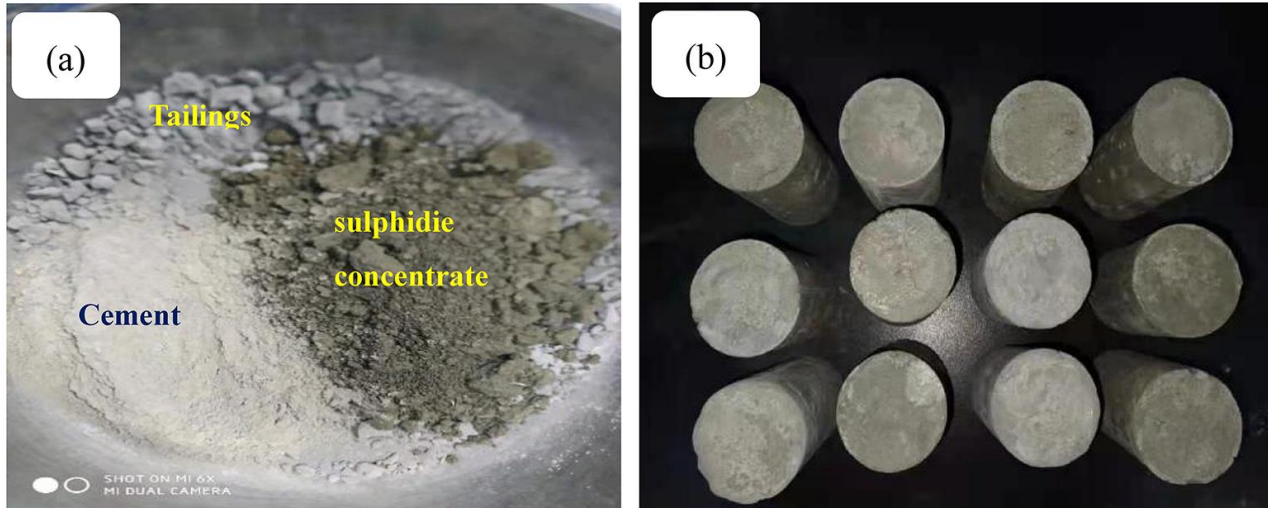


Figure 3. Experimental materials and some samples: (a) experimental materials; (b) some samples.

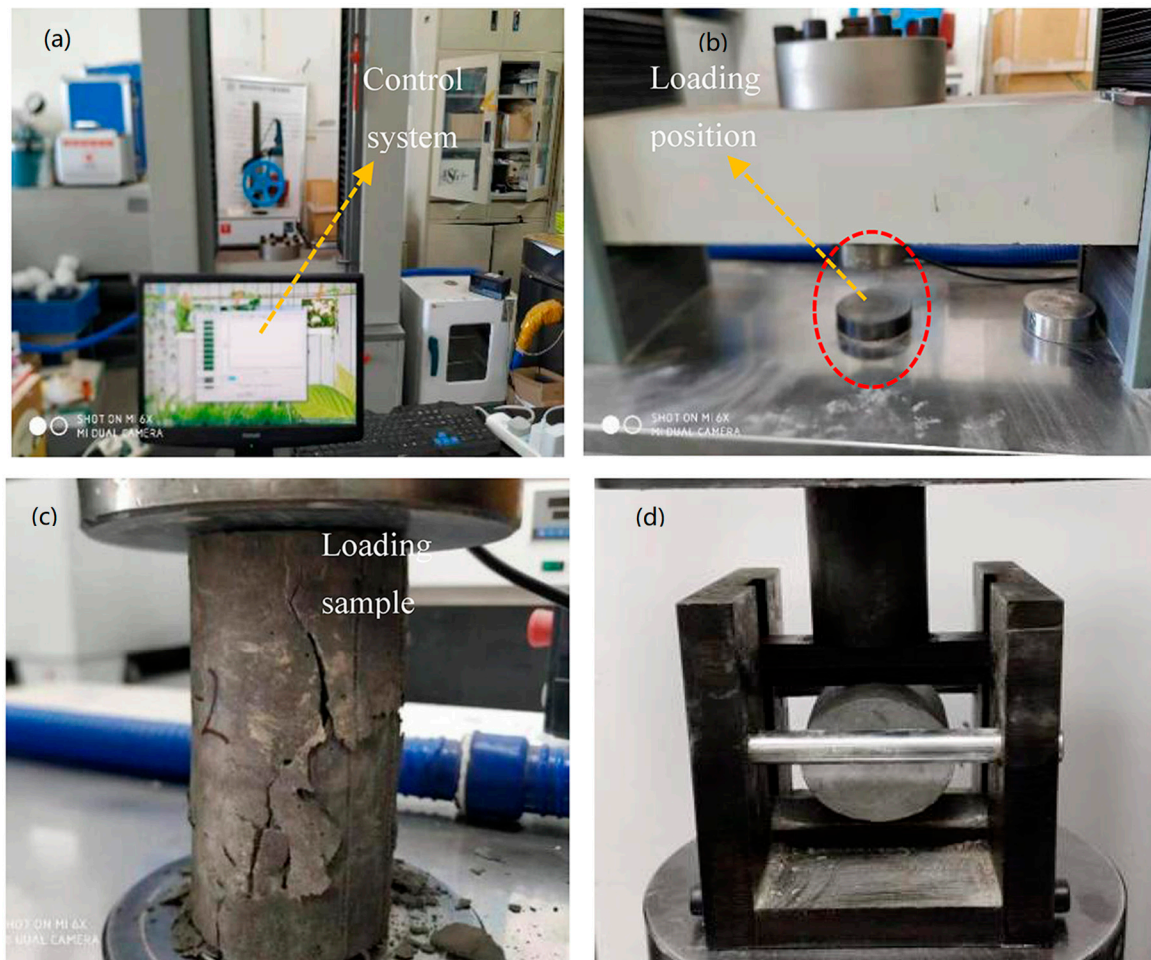


Figure 4. Experimental loading equipment: (a) control interface; (b) loading frame; (c) compressed sample; (d) split sample.

The sample size for testing the STS of CSTB remained at a diameter of 50 mm and a height of 50 mm. Samples with a curing age of 28 days were selected for testing. Similarly, each test was repeated three times, and the average value was taken as the test results.

Prior to evaluating the mechanical properties of the cemented backfill, it is essential to assess the flow properties of the filling slurry. The flow parameters of the filling slurry are tested by using the NLD-3 mortar flow meter (HUAHENG Inc., Cangzhou, China). Secondly, the microstructure was analyzed via scanning electron microscopy (SEM) (JEOL Ltd., Tokyo, Japan) to reveal how fiber and sulfur affect the mechanical properties of CSTB. The description of the flow performance test and scanning electron microscope test have been discussed in previous research [8]. In addition, the scanning electron microscope (SEM) device utilized in this study was the JSM-6510A model, with a resolution of 6 nm and a maximum acceleration voltage of 30 kV.

3. Results and Analysis

3.1. Flow Performance of Sulfur Tailings Filling Slurry

The fluidity parameters of tailings slurry were tested with NLD-3 mortar fluidity tester, the fluidity of slurry was evaluated according to the test method specified in GB/T 2419-2005 “Determination Method of Cement Mortar Fluidity”, and the changing characteristics of slurry flow performance were revealed. Figure 5 illustrates the fluidity of the no-fiber-addition group, the single-type fiber-addition group, and mixed fiber-addition group. From Figure 5a, there is a noticeable correlation between the rise in sulfur content and the increase in fluidity. This phenomenon can be attributed to the higher density of sulfide concentrate when compared to tailings. With a constant mass concentration, an increase in sulfide concentration results in a reduced volume fraction of the sulfur tailings slurry, thereby contributing to an enhancement in flow performance [9]. Figure 5b shows that the fluidity shows a trend of continuous decrease as fiber content increases, which illustrates that the addition of the two fibers exerts an adverse effect on the fluidity. In addition, when both types of fibers are added in a mixed manner, its fluidity parameters are similar to those with the separate addition of the two fibers. This illustrates that the adding method does not affect the flow performance of slurry; this is shown in Figure 5c.

The fibers in the slurry interweave to form a mesh-like structure, which greatly diminishes the slippage flow effect of tailings particles. Consequently, this phenomenon negatively impacts the flow performance of slurry [27]. To examine the impact of fiber content on the fluidity of slurry, the relationship between slurry fluidity and fiber content was fitted using an exponential function. The results are presented in Table 6 [8]. The correlation coefficients in Table 6 indicate that this result effectively describes the mathematical relationship between the two.

Table 6. Fluidity fitting model of filler slurry.

Fiber Type	Fiber Length/mm	Fitting the Model	R ²
Polypropylene	3	$y = 17.97 + 3.08 \cdot \exp(-4.87 \cdot x)$	0.930
Polypropylene	12	$y = 18.47 + 2.63 \cdot \exp(-4.93 \cdot x)$	0.951
Glass	3	$y = 17.96 + 3.35 \cdot \exp(-3.14 \cdot x)$	0.934
Glass	12	$y = 17.96 + 3.11 \cdot \exp(-4.22 \cdot x)$	0.947

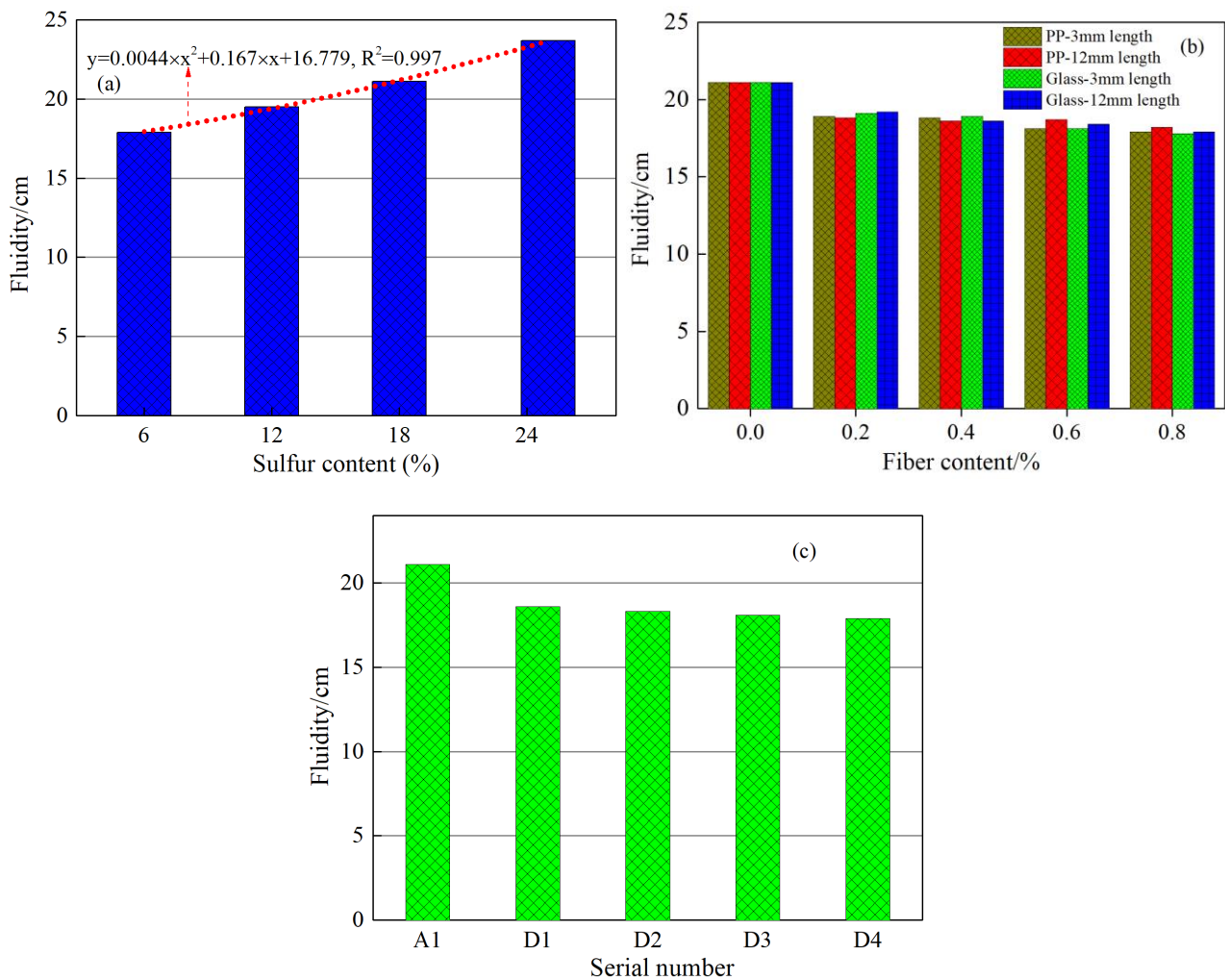


Figure 5. Fluidity parameters of sulfur tailings filling slurry: (a) unadded fiber; (b) add polypropylene and glass fiber; (c) polypropylene and fiberglass are mixed.

3.2. Influence of Sulfur Content on Mechanical Properties of Cemented Sulfur Tailings Backfill

1. Uniaxial compressive strength

Figure 6 illustrates the relationship between UCS and the curing age. In Figure 6, the numbers on the bar chart represent the specific value of the UCS, while the percentages represent the magnitude of the increase or decrease in the UCS of the CSTB. The UCS of CSTB exhibits an increasing trend followed by a decreasing trend, reaching its maximum at a sulfur content of 12%. Moreover, the impact of sulfur content on the UCS of CSTB is significantly different in different curing ages. As observed in Figure 6, an increase in sulfur content from 6% to 12% resulted in strength enhancements of 35.9%, 34.9%, 19.4% and 12.3% for samples at different curing ages (7, 14, 28 and 56 days). However, when the sulfur content increased from 12% to 25%, the strength of samples decreased by 84.3%, 25.4%, 21.3% and 41.6%, respectively. Therefore, when within the critical value range (7 and 14 days), an increase in sulfur content enhances the strength of CSTB. However, beyond the critical range, an elevated sulfur content leads to a substantial reduction in both the early and late strength of CSTB.

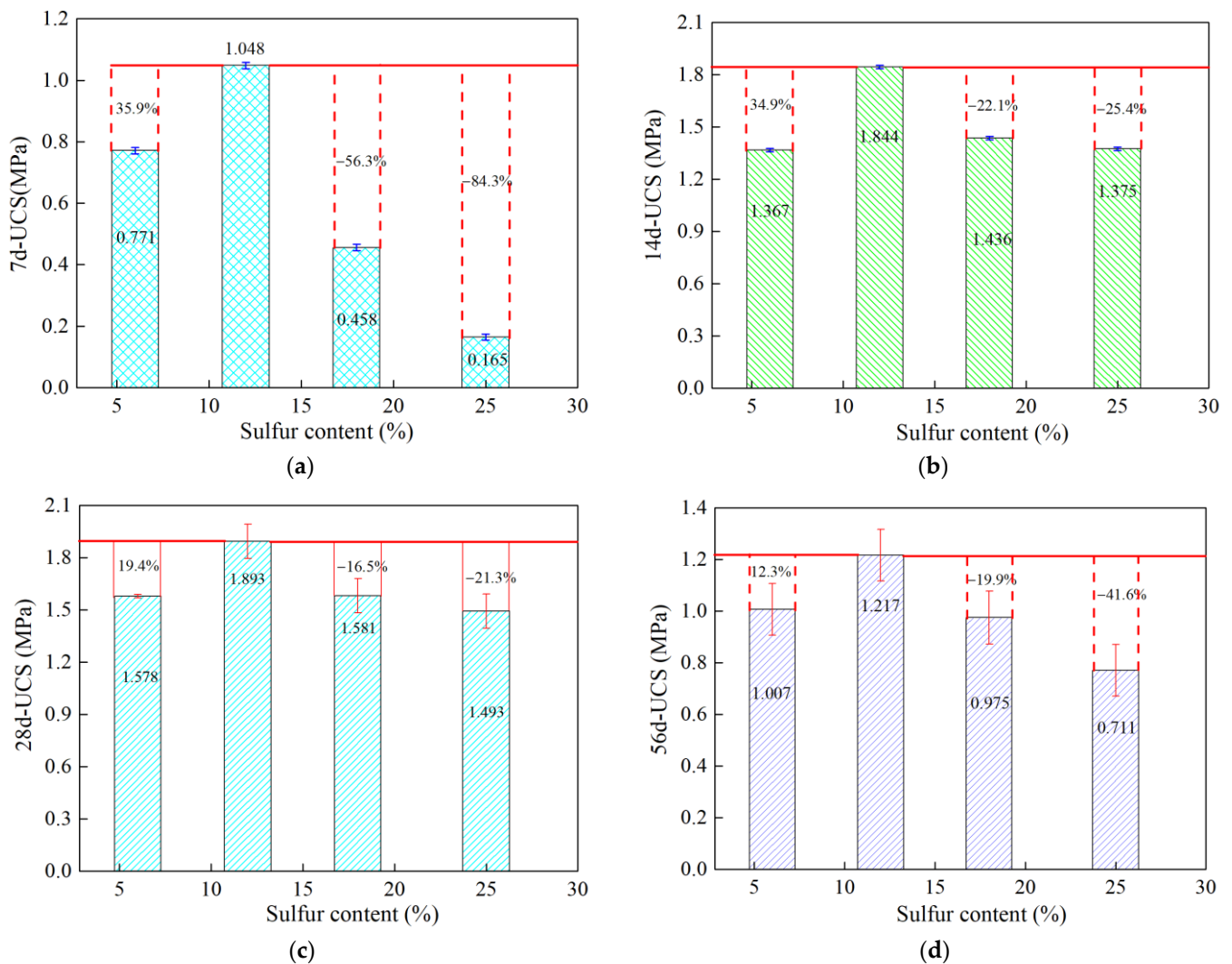


Figure 6. Uniaxial compressive strength of cemented sulfur tailings backfill in terms of differing sulfur contents. (a) 7d-UCS; (b) 14d-UCS; (c) 28d-UCS; (d) 56d-UCS.

2. Splitting tensile strength

Here, samples with a curing period of 28 days were selected for analysis. Figure 7 illustrates the variation of STS of CSTB at various sulfur content levels. In Figure 7, the numbers on the bar chart represent the specific value of the STS, while the percentages represent the magnitude of the increase or decrease in the STS of the CSTB. This indicates that the STS exhibits a similar trend to the compressive strength, reaching its maximum value at a sulfur content of 12%. It increased by 86.8% prior to reaching a sulfur content of 12%. However, thereafter, a decrease of 37.1% was observed. Therefore, within a certain range, an increase in sulfur content is beneficial for improving the splitting tensile strength. However, it also results in the loss in STS of CSTB when it reaches the critical sulfur content value. The findings of this experiment align with the research conclusions of other scholars [9,14] regarding the UCS and STS characteristics of CSTB. This consistency signifies the reliability of the test's research outcomes.

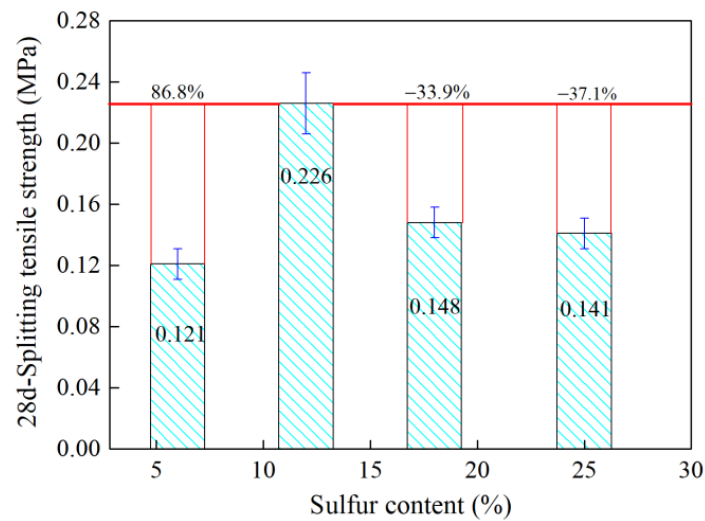


Figure 7. Splitting tensile strength of cemented sulfur tailings backfill with different sulfur contents.

3.3. Influence of Fiber on Uniaxial Compressive Strength of CSTB

1. The influence of fiber content

Figure 8 shows that when curing age is 7 days, the UCS exhibited a consistent increase as the fiber content rises. However, for other curing ages, the UCS exhibited an initial increase followed by a decrease. At 0.6% fiber content, the UCS of fiber-reinforced cemented sulfur tailings backfill (FRCSTB) reached its maximum value. With a polypropylene fiber length of 3 mm and content of 0.6%, the UCS of FRCSTB exhibits subsequent increases of 45.8%, 14.1%, 31.8%, and 80.1% with the progression of curing age. Similarly, when the polypropylene fiber length and content are 12 mm and 0.6%, respectively, the UCS of FRCSTB increases by 41.9%, 27.5%, 30.9% and 55.4% successively. Moreover, using glass fibers with lengths of 3 mm and contents of 0.6% leads to successive enhancements in the UCS of FRCSTB by 56.1%, 15.1%, 36.4% and 90.4%. When the glass fiber length and content are 12 mm and 0.6%, respectively, the UCS of FRCSTB increases by 73.4%, 31.1%, 41.7% and 60.9%, respectively. Therefore, the two types of fiber are beneficial to the UCS of FRCSTB, especially as they greatly improve the late UCS of FRCSTB. Notably, the 12 mm glass fiber exhibits the most effective improvement on the late UCS of FRCSTB. Moreover, the UCS of FRCSTB cured for 56 days decreased by 38.3% compared to FRCSTB cured for 28 days. However, at 0.6% fiber content, for the groups with added 3 mm or 12 mm polypropylene fiber and glass fiber, the UCS only decreased by 30.9%, 26.8%, 13.7% and 29.9%, respectively. It can be concluded that the polypropylene fiber and glass fiber are beneficial for improving the UCS of FRCSTB, and the glass fiber with 3 mm length has the best inhibition effect.

To investigate the correlation between the UCS and fiber content, samples with curing ages ranging from 7 to 56 days and fiber content varying from 0% to 0.6% were selected for analysis. To assess the impact of fiber content on the UCS of FRCSTB, three mathematical functions, namely exponential, linear, and polynomial functions, were selected to model the relationship between the UCS and fiber content. The corresponding results are listed in Table 7.

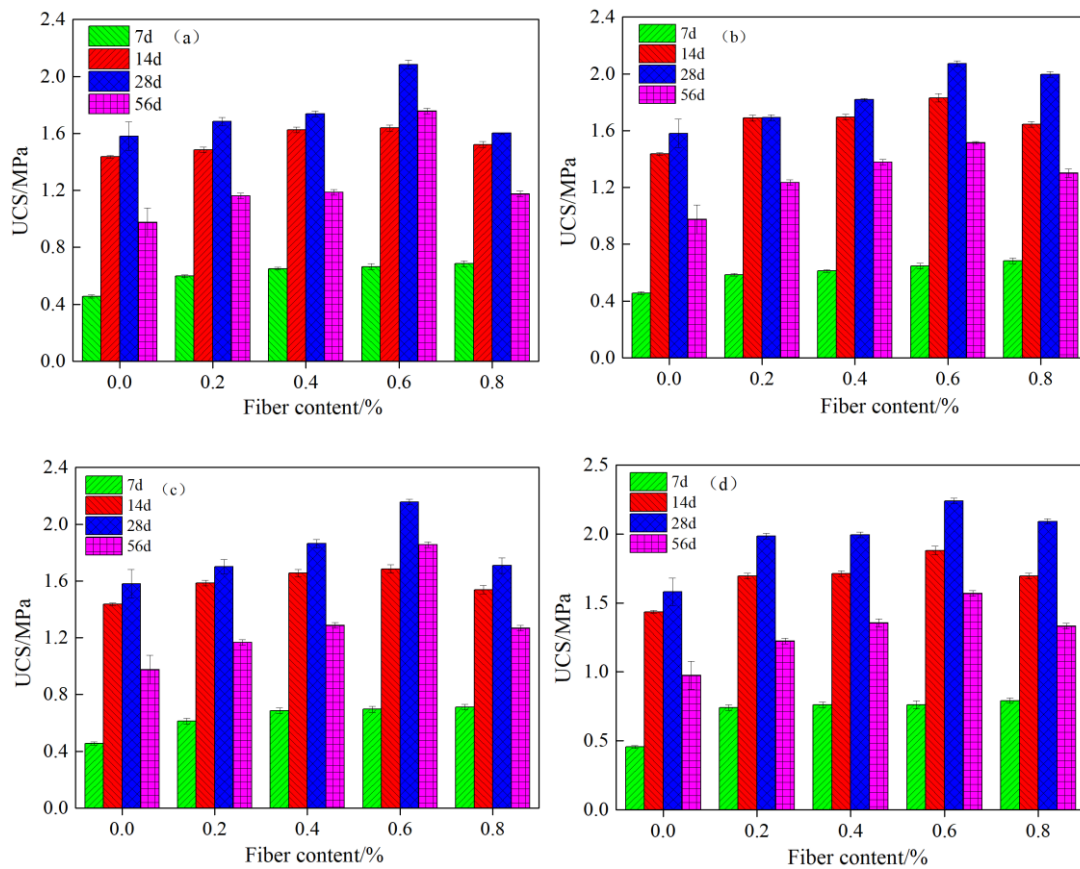


Figure 8. The relationship between UCS and fiber content of fiber-reinforced CSTB at different curing ages. (a) 3 mm length PP fiber; (b) 12 mm length PP fiber; (c) 3 mm length Glass fiber; (d) 12 mm length Glass fiber.

Table 7. Fitting model between UCS and fiber content of fiber-reinforced CSTB.

Fiber Type	Fiber Length/mm	Curing Age/d			
		7 d	14 d	28 d	56 d
PP fiber	3	$y = 0.820x - 0.800x^2 + 0.459$ $R^2 = 0.986$	$y = 0.372x + 1.434$ $R^2 = 0.865$	$y = 1.538x^2 - 0.142x + 1.598$ $R^2 = 0.876$	$y = 2.388x^2 - 0.249x + 1.010$ $R^2 = 0.781$
PP fiber	12	$y = 0.656x - 0.594x^2 + 0.462$ $R^2 = 0.908$	$y = 0.595x + 1.484$ $R^2 = 0.808$	$y = 0.894x^2 + 0.262x + 1.586$ $R^2 = 0.987$	$y = -0.769x^2 + 1.343x + 0.981$ $R^2 = 0.988$
Glass fiber	3	$y = 0.945x - 0.913x^2 + 0.457$ $R^2 = 0.998$	$y = 1.712 - 0.276 \cdot \exp(-3.866x)$ $R^2 = 0.952$	$y = 1.081x^2 + 0.295x + 1.585$ $R^2 = 0.947$	$y = 0.944 - 0.066 \cdot \exp(4.360x)$ $R^2 = 0.942$
Glass fiber	12	$y = 0.762 - 0.306 \cdot \exp(0.762x)$ $R^2 = 0.999$	$y = 0.676x + 1.479$ $R^2 = 0.853$	$y = 0.995x + 1.652$ $R^2 = 0.878$	$y = 0.957x + 0.994$ $R^2 = 0.982$

2. The influence of fiber length and fiber type

Figure 9 illustrates the correlation between the UCS of FRCSTB and the fiber length. Similarly, Figure 10 displays the relationship between the UCS of FRCSTB and fiber type. In Figure 9a, the UCS of FRCSTB with glass fiber added at 7 days, 14 days and 28 days increases as the fiber length increases, considering various fiber content levels. In Figure 9b, the UCS of FRCSTB with polypropylene fiber added at 14 days and 28 days also increased as the fiber length increased with 0.4% and 0.8% fiber content. However, at 56 days, the UCS of FRCSTB with glass fiber or polypropylene fiber decreased, as the fiber length increased with 0.6% fiber content, which may be caused by the fiber entangling and cohesive agglomeration. Therefore, the augmentation of fiber length contributes to the enhancement of mechanical characteristics in FRCSTB. However, the fiber content, fiber

uniform distribution and fiber type also influence the effect of fiber length. As shown in Figure 10, it is evident that the UCS of FRCSTB with glass fiber surpasses that of FRCSTB with polypropylene fiber across different fiber contents and lengths, underscoring the significance of fiber type in shaping the mechanical behavior of FRCSTB. This discrepancy can be attributed to the superior tensile strength and elastic modulus exhibited by glass fibers in comparison to polypropylene fiber, thereby rendering glass fiber more effective in reinforcing the FRCSTB [27].

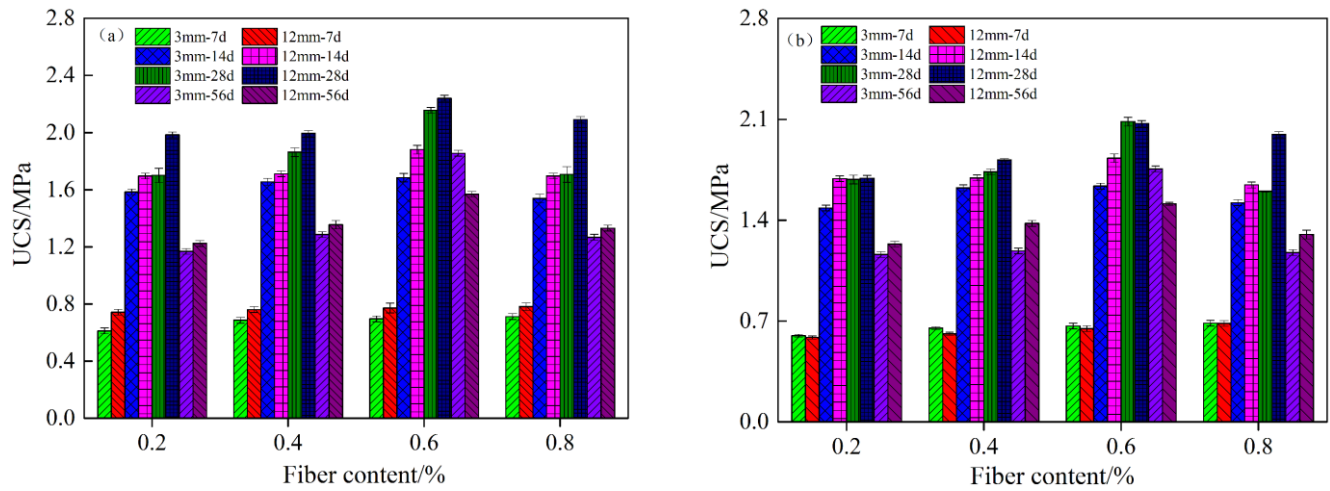


Figure 9. Relationship between the UCS of fiber-reinforced CSTB and fiber length. (a) Glass fiber; (b) polypropylene fiber.

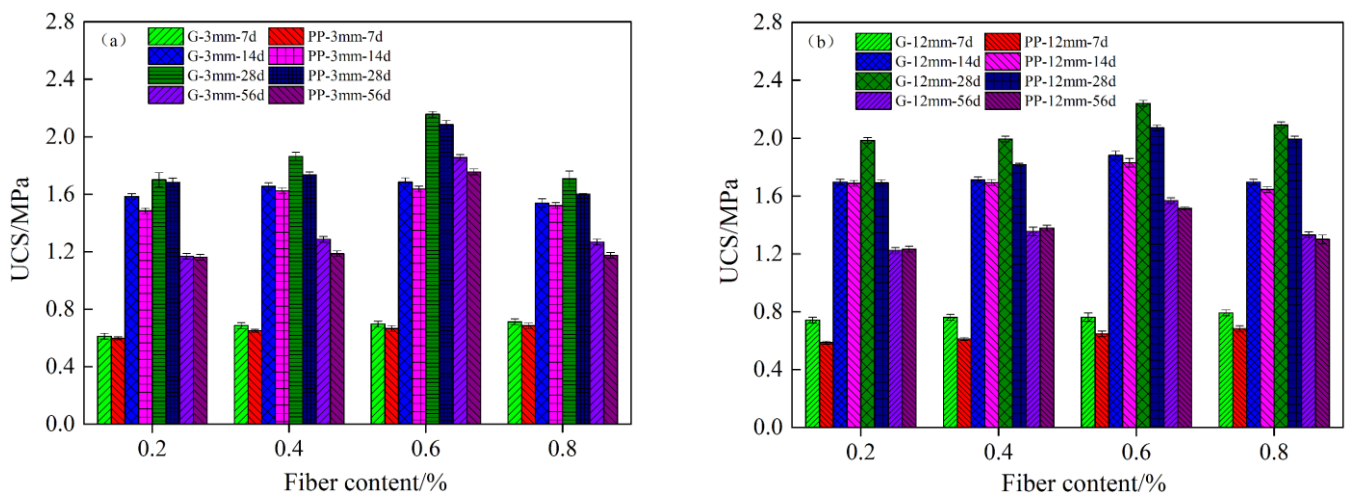


Figure 10. Relationship between compressive strength of fiber-reinforced CSTB and fiber type. (a) Fiber length, 3 mm; (b) fiber length, 12 mm.

3. The influence of fiber adding method

Figure 11 shows the UCS of FRCSTB added with both glass fiber and polypropylene fiber. The results indicate that the mixed addition of polypropylene fiber and glass fiber can also effectively increase the UCS of FRCSTB. However, it is noteworthy that the UCS will also decrease once the fiber content is more than 0.6%. Moreover, its UCS was lower than that of the FRCSTB added with only one type of fiber. Therefore, adding only one type of fiber is more beneficial for the increase in USC of CSTB.

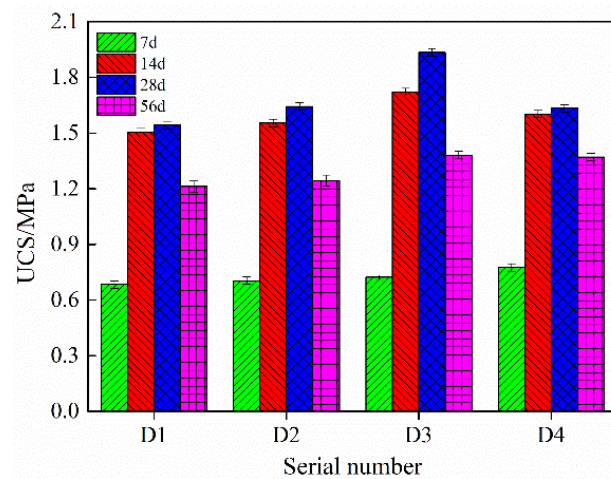


Figure 11. Relationship between the UCS of fiber-reinforced CSTB and fiber adding method.

3.4. Influence of Fiber on Splitting Tensile Strength of Cemented Sulfur Tailings Backfill

1. The influence of fiber content and fiber length

Figure 12 presents the impact of fiber length and content on the STS of CSTB at a curing age of 28 days. The addition of polypropylene fiber or glass fiber is advantageous for enhancing the STS of CSTB. However, it is noteworthy that when the fiber content reaches 0.6%, the STS starts to decline. Therefore, a fiber content of 0.6% is found to be the optimum. Furthermore, with the fiber content reaches 0.6%, the STS of FRCSTB experiences a notable increase, specifically by 203%, 205%, 205% and 219% when polypropylene fiber and glass fiber values are 3 mm and 12 mm. However, the 28 d UCS of FRCSTB only increased by 31.8%, 30.9%, 36.4% and 41.7%. These results suggest that fiber addition exerts a more significant influence on the STS of FRCSTB. Moreover, the enhancement of fiber length also proved to be advantageous in improving the STS of CSTB, especially at 0.2% and 0.4% fiber content, with the greatest impact on the STS of CSTB.

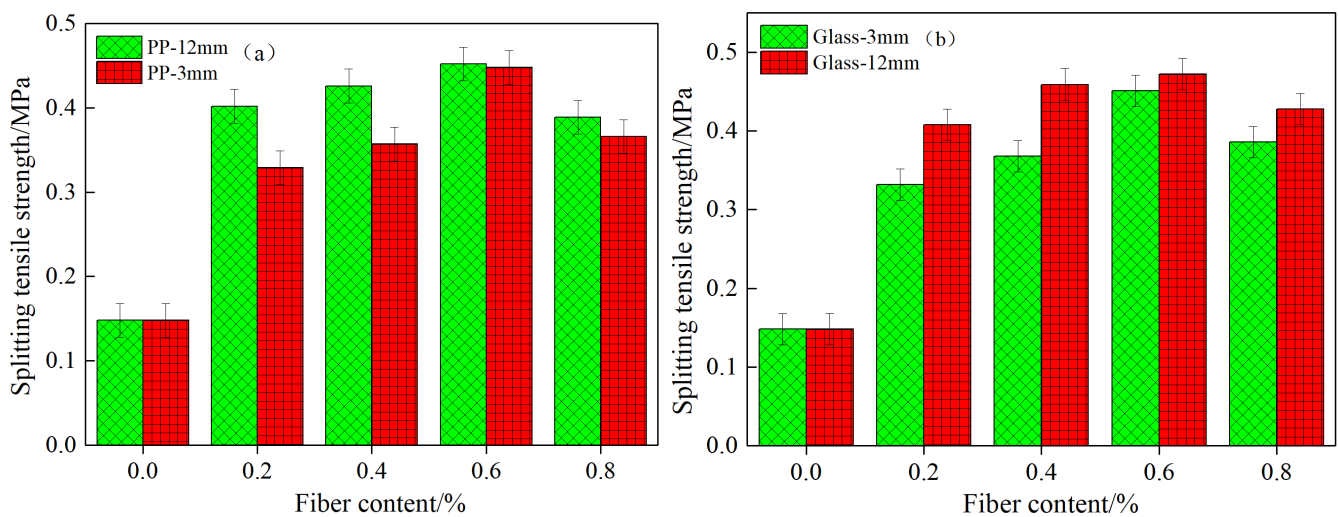


Figure 12. Relationship between tensile strength and fiber content and length of fiber-reinforced CSTB. (a) polypropylene fiber; (b) glass fiber.

2. The influence of fiber type and fiber adding method

Figure 13 shows the relationship between the STS of FRCSTB and the fiber type and fiber addition method. In Figure 13a, glass fiber is more beneficial for improving tensile strength under the conditions of various fiber contents. Especially, when the fiber length

is 12 mm, the CSTB with added glass fiber exhibits higher tensile strength. Therefore, the addition of high-performance fiber is very important.

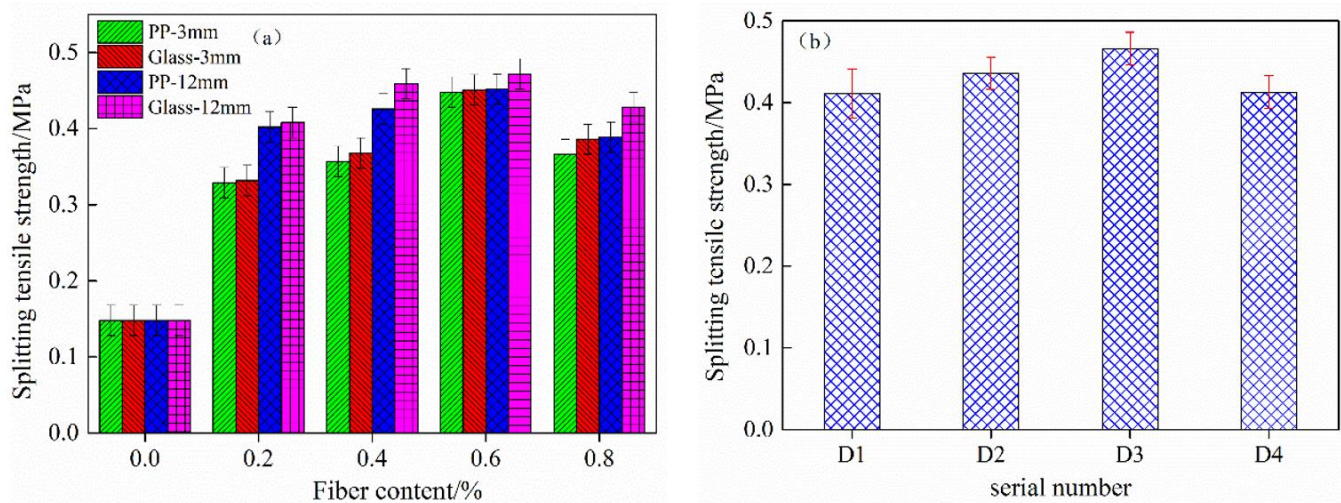


Figure 13. Relationship between tensile strength of fiber-reinforced CSTB and fiber type and adding method: (a) fiber type; (b) fiber adding method.

Figure 13b illustrates that the combined inclusion of polypropylene fiber and glass fiber is also beneficial to the UCS of CSTB. However, it should be noted that the tensile strength experiences a decline as the fiber content surpasses 0.6%. The tensile strength of backfill numbered D1, D2, D3 and D4 is 0.411 MPa, 0.436 Pa, 0.466 MPa and 0.413 MPa, the UCS of backfill numbered B5, B6, B7 and B8 is 0.402 MPa, 0.426 MPa, 0.452 MPa and 0.389 MPa, and the UCS of the backfill numbered C5, C6, C7 and C8 is 0.408 MPa, 0.459 MPa, 0.472 MPa and 0.428 MPa at 28 days. Therefore, the tensile strength enhancement effect of the mixed fiber addition method is lower than that of glass fiber alone but better than that of polypropylene fiber alone.

3.5. Microstructural Analysis of CSTB and Fiber-Reinforced CSTB

SEM was employed to examine the microstructure characteristics of CSTB and FRCSTB. Figure 14 illustrates the microstructure of CSTB at various sulfur contents after a curing age of 14 days. It can be seen that, with sulfur content increasing, significant changes occur in the hydration products and pore structure. In terms of pore structure, as the sulfur content increases, it initially decreases and then increases, reaching its maximum at a sulfur content of 12%. This can also explain the reason for the decrease in strength due to excessive sulfur content. For 6% sulfur content, C–S–H gel microaggregates and elongated cubic secondary gypsum can be identified, but no observable nearly prism-shaped acicular ettringite is present. For 12% sulfur content, hydration products are visible everywhere, and the presence of slender cube shaped secondary gypsum can still be observed. Finally, a significant amount of gypsum and ettringite was generated when sulfur content exceeded 18%. Once the pyrite in the CSTB was exposed to air and water, an oxidation reaction occurs, leading to the formation of acid and sulfate (Equation (1)). The formation of acid can contribute to C–S–H gel decalcification, resulting in the reduction in existing hydration products, thereby weakening the strength of the CSTB [28]. At the same time, a sustained response occurs in oxide, C3A and $\text{Ca}(\text{OH})_2$, resulting in the formation of the expanded phase products, ettringite and secondary gypsum (Equations (2) and (3)). The growth and expansion of the swelling phase product leads to the compression of the surrounding hydrated product structure in CSTB, resulting in increased tensile stress within the material. When the cohesion between the hydration products is not enough to resist tensile stress, obvious cracks will occur inside the CSTB (Figure 14c), which reduces the strength [29,30]. Hence, within the range of 6% to 12% sulfur content, the formation of secondary gypsum, resulting from pyrite oxidation, contributes to decreased

porosity and the enhanced compactness of CSTB. This leads to improved UCS and STS of CSTB. However, when sulfur content exceeds 12%, the excessive secondary gypsum causes the CSTB to expand in volume, thus weakening the UCS and STS of CSTB [30]. In addition, excessive acid and sulfate leads to a large reduction in the quantity of C-S-H gel when sulfur content exceeds 12%, resulting in an obvious pore structure inside the CSTB (Figure 14d), which also reduces the mechanical properties of the CSTB [28,31].

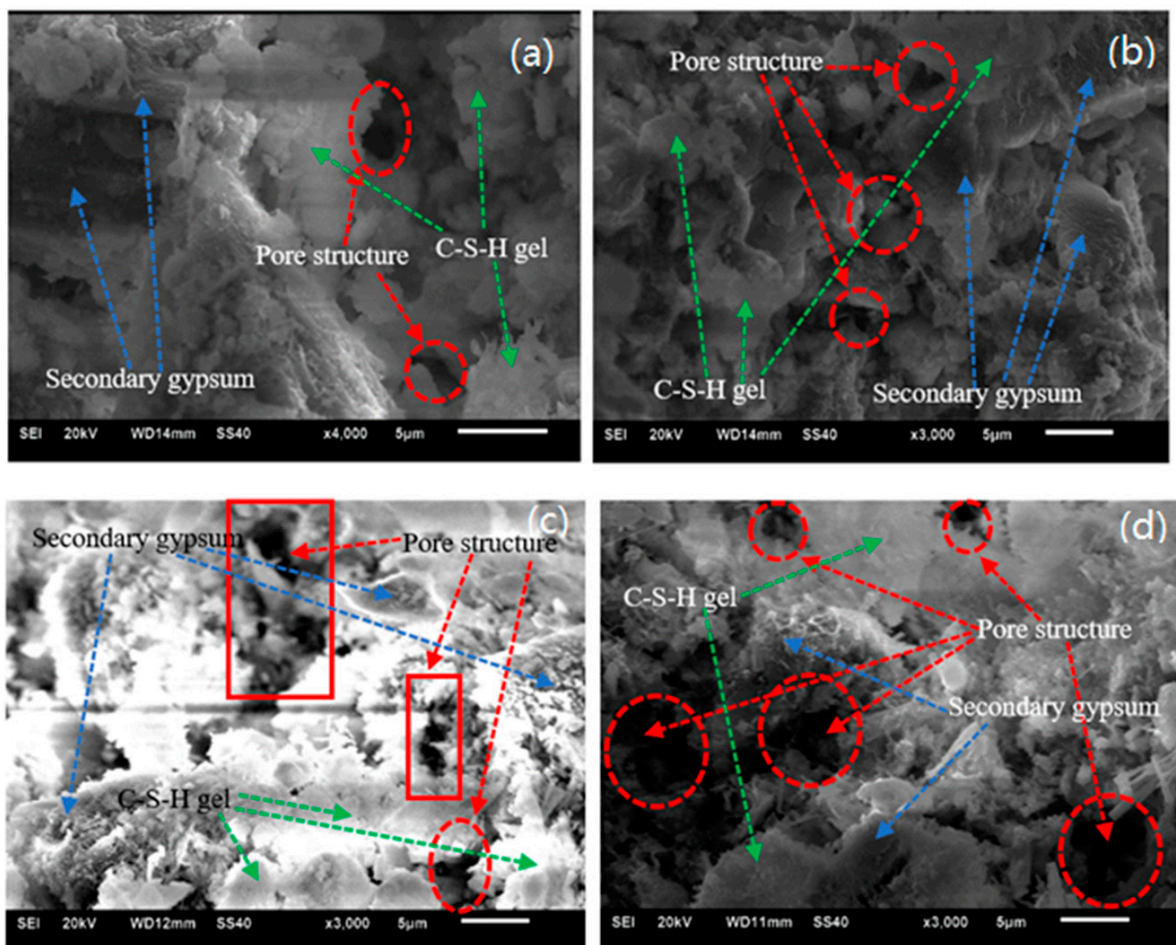
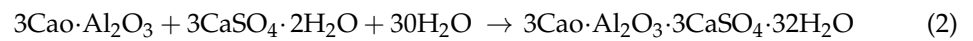
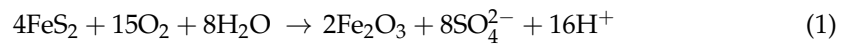


Figure 14. Microstructure characteristics of CSTB with different sulfur contents. (a) sulfur content is 6%; (b) sulfur content is 12%; (c) sulfur content is 18%; (d) sulfur content is 25%.

Figure 15 shows the surface SEM images of polypropylene fiber and glass fiber inside the CSTB. In Figure 15, the hydration products are scattered on the fiber surface, intertwining with mortar and forming adhesion, which enhances the strength of FRCSTB. Meanwhile, the process of hydration produces compounds that effectively occupy the gaps between the fiber and cement-tailing matrix, thus further improving the bonding force between the fiber and mortar matrix. Therefore, the stress is dispersed by the fibers in the fiber-reinforced CSTB when the samples are subjected to uniaxial loading, thus improving the mechanical properties and effectively controlling the deterioration of the strength of the CSTB in later stages.

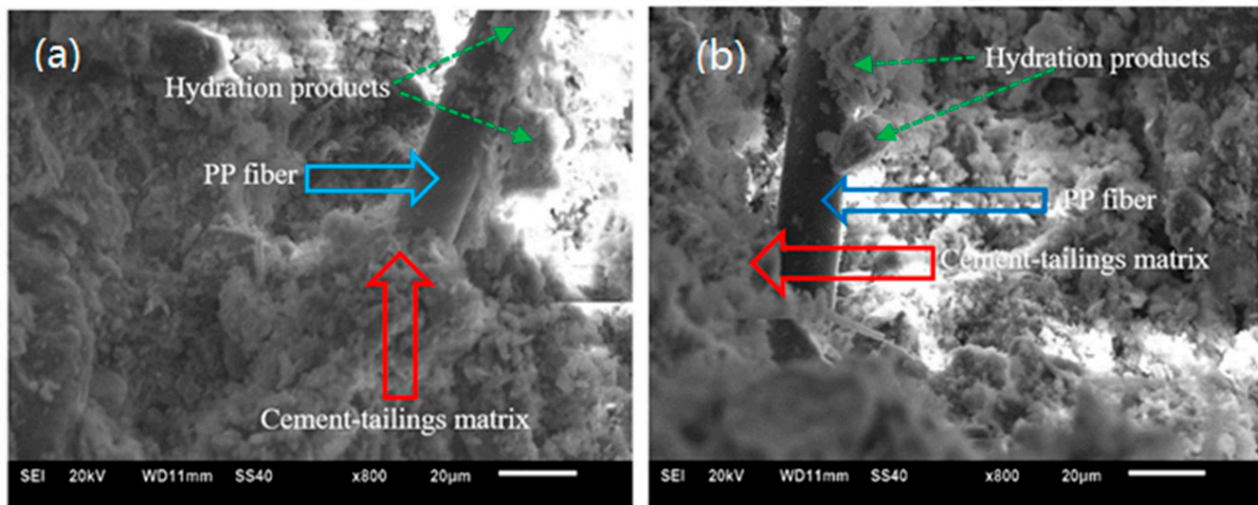


Figure 15. SEM image of the fiber surface inside the fiber-reinforced CSTB. (a) polypropylene fiber; (b) glass fiber.

Moreover, the fibers effectively inhibit the propagation of cracks, as shown in Figure 16. There are obvious pore and crack structures in the CSTB samples without fiber and hydration products, such as sub-gypsum and C-S-H gel, which are also produced on the surface of the samples. In Figure 16b, there are no obvious cracks and pore structures inside the CSTB containing glass fiber. This observation indicates that fiber can effectively prevent the formation and expansion of pores and cracks, thereby enhancing the physical properties of the CSTB.

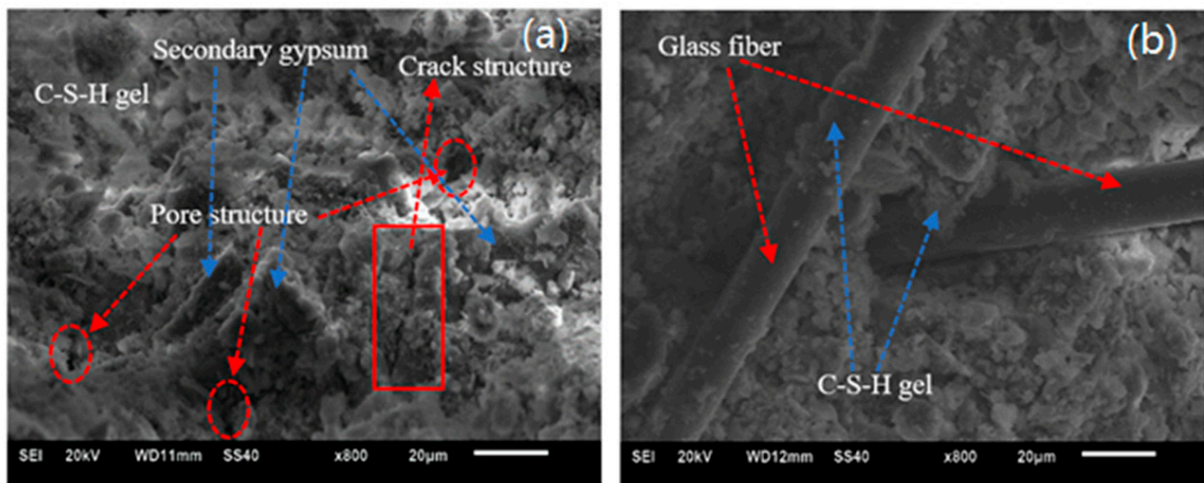


Figure 16. Reinforcement mechanism of fiber on CSTB. (a) unreinforced CSTB sample; (b) glass fiber-reinforced CSTB sample.

3.6. Effect of Curing Age on Compressive Strength of Fiber-Reinforced CSTB

Figure 17 presents the impact of the curing age on the UCS of FRCSTB. In Figure 17, the UCS of FRCSTB decreases after initially increasing with increasing fiber content. In addition, according to the strength growth curve of FRCSTB, the strength growth of CSTB can be categorized into three stages:

1. Rapid growth stage. When the curing age is 7 d~14 d, there is an obvious linear correlation between the UCS and the curing age. This is because the C-S-H gel and sub-gypsum are generated on the surface of CSTB sample at early-stage curing, thus rapidly improving the UCS of CSTB.

2. Stable increase of strength. The slope of the UCS growth curve of the CSTB decreases significantly at 14~28 d of curing age, indicating that the UCS growth rate is significantly reduced. This is because the generated acid and sulfate lead to a decrease in the amount of C-S-H gel after curing for more than 14 d, which inhibits the UCS of CSTB and thus slows down the growth rate of the UCS of CSTB.
3. Compressive strength decline stage. As the curing age surpasses 28 days, the UCS of CSTB experiences a reduction in the progression of curing age. Combined with the oxidation reaction of pyrite, it can be seen that the internal erosion of acid and sulfate ions and the expansion characteristics of secondary gypsum are the main reasons for the strength decline in CSTB at a later stage.

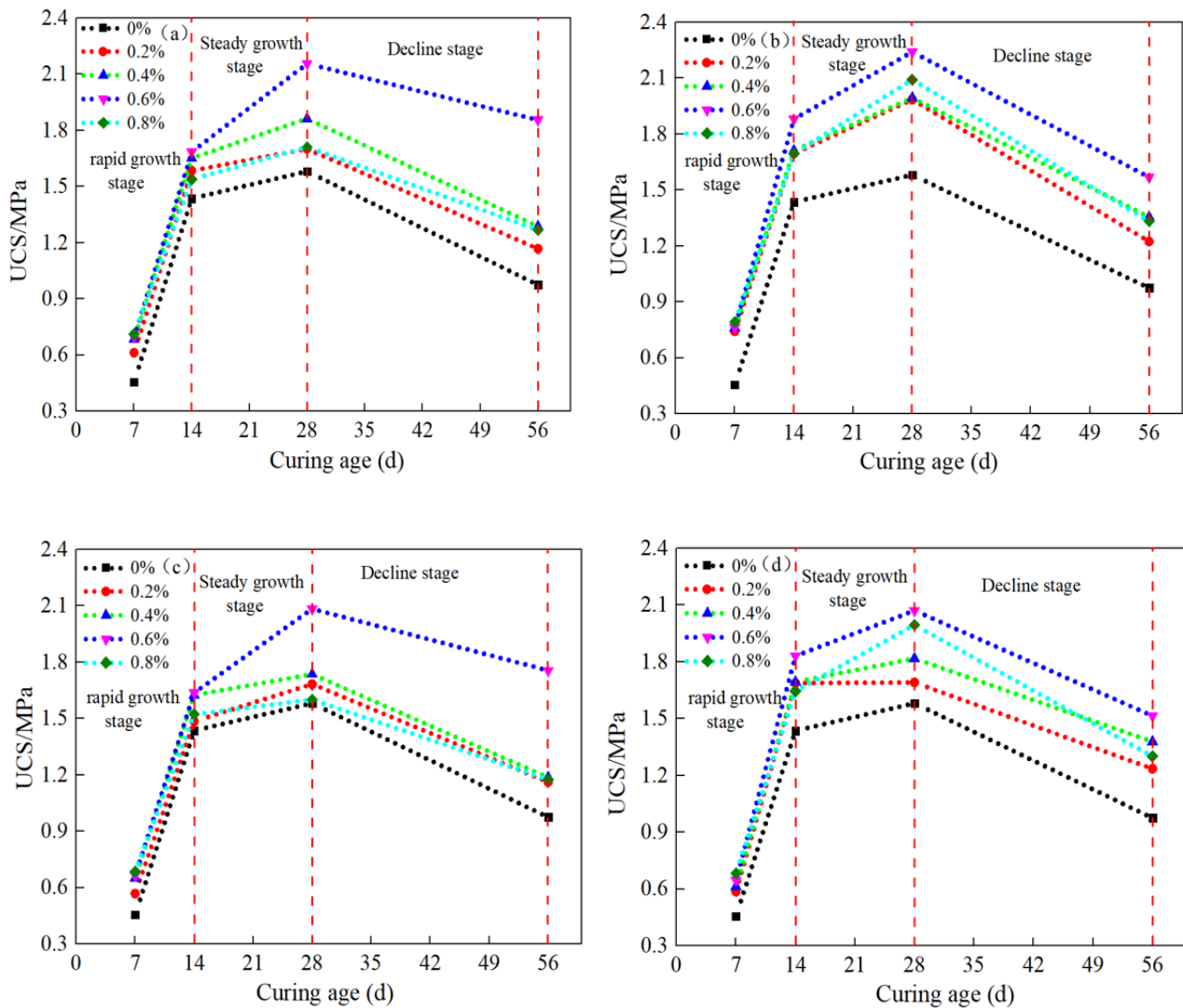


Figure 17. The relationship between the compressive strength of fiber-reinforced CSTB and the curing age. (a) 3 mm length glass fiber; (b) 12 mm length glass fiber; (c) 3 mm length PP fiber; (d) 12 mm length PP fiber.

Moreover, the UCS of FRCSTB exhibits a notable improvement compared to that of conventional CSTB when the curing period is 56 d, indicating that the UCS significantly increases and strength deterioration is limited after adding fibers. Additionally, the increase in UCS of CSTB remains consistent regardless of the fiber type, indicating that the change in fiber types will not have an impact on the growth law of UCS.

4. Conclusions

In this study, a systematic investigation was conducted to examine the impact of fiber type, content, length and the fiber addition method on the mechanical properties and flow performance of CSTB. The experimental research yielded the following research conclusions:

1. The addition of fibers restricts the flowability of the tailings slurry. Fluidity exhibits an exponential decrease with increasing fiber content. Moreover, the UCS and STS of CSTB initially increase and then decrease with increasing sulfur content, reaching a maximum value at 12% sulfur content.
2. When the fiber content ranges from 0% to 0.6%, adding fiber can enhance the mechanical properties of the CSTB. The strengthening effect of glass fiber on compressive strength is higher than that of polypropylene fiber, and the impact of fiber mixing on compressive strength is not as good as that of a single addition.
3. Glass fiber demonstrates a greater enhancement in tensile strength compared to polypropylene fiber. Additionally, the improvement in the UCS of CSTB through mixed fiber addition is obviously less effective than that through single fiber addition, but the enhancement in STS surpasses that achieved by using polypropylene fiber alone.
4. Augmenting fiber length also improves the STS of CSTB, with glass fiber exhibiting a superior reinforcing effect compared to polypropylene fiber. The addition of mixed fibers has a more positive impact on enhancing the STS than separate additions, particularly in the case of polypropylene fiber.
5. Below the critical content of 12% sulfur, the presence of secondary gypsum and ettringite crystals within the pores enhances overall density and leads to higher strengths. However, exceeding the critical content results in internal erosion caused by acid and sulfuric acid ions, as well as the expansion characteristics of sub-gypsum, leads to the formation of numerous pore and crack structures within CSTB. Consequently, the UCS and STS of CSTB are diminished.
6. This study provided detailed analysis of the influence of fiber content, fiber type and the fiber addition method on the physical and flow properties of CSTB, resulting in valuable research findings. In the future research, the following two aspects of research work will be emphasized: (1) focusing on the influence of fiber content, fiber type and method of fiber addition on the rheological characteristics of the CSTB and establishing a rheological parameter prediction model considering fiber characteristic parameters as well as (2) investigating the mechanical properties of FRCSTB under multi-field coupling conditions and constructing a damage constitutive model of CSTB under multi-field coupling conditions.

Author Contributions: Conceptualization, W.L. and S.Y.; methodology, W.L.; software, Y.H.; validation, M.Z.; formal analysis, M.Z.; investigation, Y.H.; resources, S.Y.; data curation, M.Z.; writing—original draft preparation, W.L.; writing—review and editing, W.L.; visualization, W.L.; supervision, S.Y.; project administration, S.Y.; funding acquisition, S.Y. All authors have read and agreed to the published version of the manuscript.

Funding: This research was funded by Key Program of National Natural Science Foundation of China grant number 51734001, and Key Program of National Natural Science Foundation of China grant number 51834001.

Data Availability Statement: All data are contained within the article.

Acknowledgments: The authors thank Xin Chen for the revision and polishing of the manuscript.

Conflicts of Interest: The authors declare no conflict of interest.

References

1. Huang, S.B.; Pi, Z.J.; Cai, C.; Li, H. Utilization of high-sulfur iron ore tailings in cement mortar by considering the influence of curing temperature and tailing content. *J. Build. Eng.* **2023**, *74*, 106826. [[CrossRef](#)]
2. Li, H.; Wu, A.X.; Wang, H.J. Evaluation of short-term strength development of cemented backfill with varying sulphide contents and the use of additives. *J. Environ. Manag.* **2019**, *239*, 279–286. [[CrossRef](#)] [[PubMed](#)]
3. Qi, C.C.; Fourie, A.; Chen, Q.S.; Zhang, Q.L. A strength prediction model using artificial intelligence for recycling waste tailings as cemented paste backfill. *J. Clean Prod.* **2018**, *183*, 566–578. [[CrossRef](#)]
4. Wang, J.; Fu, J.X.; Song, W.D.; Zhang, Y.F.; Wang, Y. Mechanical behavior, acoustic emission properties and damage evolution of cemented paste backfill considering structural feature. *Constr. Build. Mater.* **2020**, *261*, 119958. [[CrossRef](#)]
5. Kongar-Syuryun, C.; Aleksakhin, A.; Khayrutdinov, A.; Tyulyaeva, Y. Research of rheological characteristics of the mixture as a way to create a new backfill material with specified characteristics. *Mater. Today* **2021**, *38*, 2052–2054. [[CrossRef](#)]
6. Liu, L.; Xin, J.; Huan, C.; Qi, C.C.; Zhou, W.W.; Song, K. Pore and strength characteristics of cemented paste backfill using sulphide tailings: Effect of sulphur content. *Constr. Build. Mater.* **2020**, *237*, 117452. [[CrossRef](#)]
7. Yin, S.H.; Hou, Y.Q.; Chen, X.; Zhang, M.Z.; Du, H.H.; Gao, C. Mechanical behavior, failure pattern and damage evolution of fiber-reinforced cemented sulfur tailings backfill under uniaxial loading. *Constr. Build. Mater.* **2022**, *332*, 127248. [[CrossRef](#)]
8. Yin, S.H.; Hou, Y.Q.; Chen, X.; Zhang, M.Z. Mechanical, flowing and microstructural properties of cemented sulfur tailings backfill: Effects of fiber lengths and dosage. *Constr. Build. Mater.* **2021**, *309*, 125058. [[CrossRef](#)]
9. Chen, H.Y.; Wu, A.X.; Wang, H.J.; Wang, Y.M. Experimental study on the strength deterioration of sulfidic paste backfill. *Chin. J. Eng.* **2017**, *39*, 1493–1497.
10. Zeng, J.; Qiu, J.R.; Zhang, J.; Qi, Y.Q.; Liu, R.T.; Jian, C.Q.; Liu, N.; Su, Y.M. Plant ash prevents acid mine drainage from sulfur-bearing tailings through multiple actions—A low-cost alkaline material. *Appl. Geochem.* **2023**, *155*, 105702. [[CrossRef](#)]
11. Jiang, G.Z.; Wu, A.X.; Li, H.; Wang, Y.M.; Wang, H.J. Long-term strength performance of sulfur tailings filling and its affecting factors. *J. Cent. South Univ. (Sci. Technol.)* **2018**, *49*, 1504–1510.
12. Ayora, C.; Chinchon, S.; Aguado, A.; Guirado, F. Weathering of iron sulfides and concrete alteration: Thermodynamic model and observation in dams from Central Pyrenees, Spain. *Cem. Concr. Res.* **1998**, *28*, 591–603. [[CrossRef](#)]
13. Yin, S.H.; Shao, Y.J.; Wu, A.X.; Wang, Y.M.; Chen, X. Expansion and strength properties of cemented backfill using sulphidic mill tailings. *Constr. Build. Mater.* **2018**, *165*, 138–148. [[CrossRef](#)]
14. Dong, Q.; Liang, B.; Jia, L.F.; Jiang, L.G. Effect of sulfide on the long-term strength of lead-zinc tailings cemented paste backfill. *Constr. Build. Mater.* **2019**, *200*, 436–446. [[CrossRef](#)]
15. Wang, S.; Song, X.P.; Chen, Q.S.; Wang, X.J.; Wei, M.L.; Ke, Y.X.; Luo, Z.H. Mechanical properties of cemented tailings backfill containing alkalinized rice straw of various lengths. *J. Environ. Manag.* **2020**, *276*, 111124. [[CrossRef](#)]
16. Ermolovich, E.A.; Ivannikov, A.L.; Khayrutdinov, M.M.; Kongar-Syuryun, C.B.; Tyulyaeva, Y.S. Creation of a Nanomodified Backfill Based on the Waste from Enrichment of Water-Soluble Ores. *Materials* **2022**, *15*, 3689. [[CrossRef](#)] [[PubMed](#)]
17. Kongar-Syuryun, C.B.; Faradzov, V.V.; Tyulyaeva, Y.S.; Khayrutdinov, A.M. Effect of activating treatment of halite flotation waste in backfill mixture preparation. *Min. Informational Anal. Bull.* **2021**, 43–57. [[CrossRef](#)]
18. Khayrutdinov, A.; Kongar-Syuryun, C.; Kowalik, T.; Faradzov, V. Improvement of the backfilling characteristics by activation of halite enrichment waste for non-waste geotechnology. *IOP Conf. Ser. Mater. Sci. Eng.* **2020**, *867*, 012018. [[CrossRef](#)]
19. Sadrolodabae, P.; Claramunt, J.; Ardanuy, M.; Fuente, A. Mechanical and durability characterization of a new textile waste micro-fiber reinforced cement composite for building applications. *Case Stud. Constr. Mat.* **2021**, *14*, e00492.
20. Sadrolodabae, P.; Claramunt, J.; Ardanuy, M.; Fuente, A. A Textile Waste Fiber-Reinforced Cement Composite: Comparison between Short Random Fiber and Textile Reinforcement. *Materials* **2021**, *14*, 3742. [[CrossRef](#)]
21. Xu, W.B.; Li, Q.L.; Tian, M.M. Strength and deformation properties of polypropylene fiber-reinforced cemented tailings backfill. *Chin. J. Eng.* **2019**, *41*, 1618–1626.
22. Chen, X.; Shi, X.Z.; Zhou, J.; Chen, Q.S. Compressive behavior and microstructural properties of tailings polypropylene fibre-reinforced cemented paste backfill. *Constr. Build. Mater.* **2018**, *190*, 211–221. [[CrossRef](#)]
23. Yi, X.W.; Ma, G.W.; Fourie, A. Compressive behavior of fiber-reinforced cemented paste backfill. *Geotext. Geomembr.* **2015**, *43*, 207–215. [[CrossRef](#)]
24. Zhou, N.; Du, E.B.; Zhang, J.X.; Zhu, C.L.; Zhou, H.Q. Mechanical properties improvement of Sand-Based cemented backfill body by adding glass fibers of different length sand ratios. *Constr. Build. Mater.* **2021**, *280*, 122408. [[CrossRef](#)]
25. Xue, G.L.; Yilmaz, E.; Song, W.D.; Cao, S. Mechanical, flexural and microstructural properties of cement-tailings matrix composites: Effects of fiber type and dosage. *Compos. Part B-Eng.* **2019**, *172*, 131–142. [[CrossRef](#)]
26. Cao, S.; Yilmaz, E.; Song, W.D. Fiber type effect on strength, toughness and microstructure of early age cemented tailings backfill. *Constr. Build. Mater.* **2019**, *223*, 44–54. [[CrossRef](#)]
27. Quan, C.Q.; Jiao, C.J.; Yang, Y.Y.; Li, X.B.; Lei, Z. Orthogonal experimental study on mechanical properties of hybrid fiber reinforced concrete. *J. Build. Mater.* **2019**, *22*, 363–370.
28. Benzaazoua, M.; Fall, M.; Belem, T. A contribution to understanding the hardening process of cemented pastefill. *Miner. Eng.* **2004**, *17*, 141–152. [[CrossRef](#)]
29. Yang, J.S. Discussion on the action duality of ettringite and its causing condition in concrete. *China Civ. Eng. J.* **2003**, *36*, 100–103.

30. Xiao, J.; Deng, D.H.; Zhang, W.N.; Zeng, Z.; Tang, X.Y. Formation of gypsum leading to the destruction of cement paste under the external sulfate attacking. *J. Build. Mater.* **2006**, *9*, 19–23.
31. He, Z.; Wang, L.; Shao, Y.X.; Cai, X.H. Effect of decalcification on C-S-H gel microstructure in cement paste. *J. Build. Mater.* **2011**, *14*, 293–298.

Disclaimer/Publisher’s Note: The statements, opinions and data contained in all publications are solely those of the individual author(s) and contributor(s) and not of MDPI and/or the editor(s). MDPI and/or the editor(s) disclaim responsibility for any injury to people or property resulting from any ideas, methods, instructions or products referred to in the content.